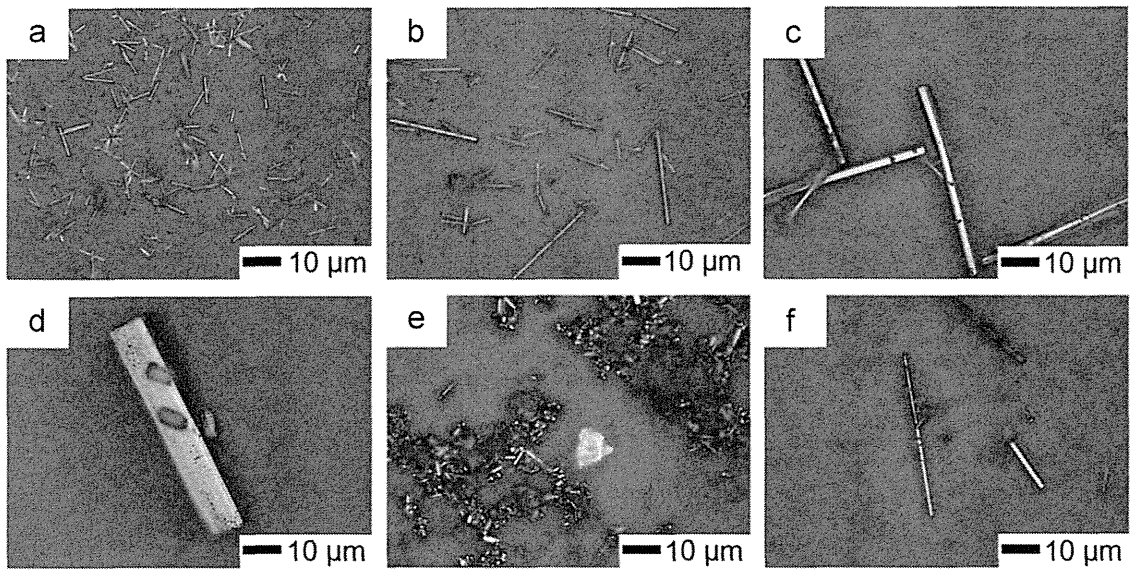

Fig. 1. Optical images of the precipitates. The compositions of mother solutions were (a) C_{60}–9 mass% C_{70}, (b) C_{60}–24 mass% C_{70}, (c) C_{60}–37 mass% C_{70}, (d) C_{60}–45 mass% C_{70}, (e) C_{60}–78 mass% C_{70}, (f) 100 mass% C_{70}.

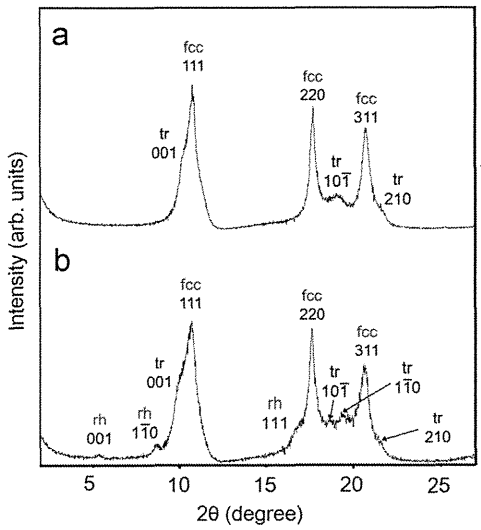

Fig. 2. XRD patterns of (a) the C_{60}NWs and (b) the C_{60}–C_{70}NWs obtained using a mother solution with a composition of C_{60}–24 mass% C_{70}.

(XRD), high-performance liquid chromatography (HPLC), Raman spectroscopy and ultraviolet–visible (UV–vis) spectroscopy.

2. Experimental

Powders of C_{60} (MTR Ltd., 99.5%) and C_{70} (MTR Ltd., 99.0%) were dissolved in toluene (WAKO JIS special grade) by ultrasonic agitation (Iuchi VS-150). The solutions were filtered using syringe filters (MITSUBA HIGH GRADE SYRINGE, Whatman 25 mm GD/X) to generate a C_{60}-saturated toluene solution and a C_{70}-saturated toluene solution.

The C_{60}- and C_{70}-saturated toluene solutions were mixed in various ratios to form C_{60}–C_{70} two-component mother solutions. The mixing ratios were (10.0 mL [C_{60}], 0 mL [C_{70}]), (9.5, 0.5), (9.0, 1.0), (8.5, 1.5), (8.0, 2.0), (7.0, 3.0), (6.0, 4.0), (5.0, 5.0), (4.0, 6.0), (3.0, 7.0), (2.0, 8.0), (1.5, 8.5), (1.0, 9.0), (0.8, 9.2), (0.6, 9.4), (0.5, 9.5), (0.4, 9.6), (0.2, 9.8) and (0, 10.0).

The temperature of each mother solution, stored in glass bottles (volume: 30 mL, inner diameter: 27 mm), was set to 15 °C using a water bath (AS ONE UCT-1000). 10 mL of 2-propanol (WAKO JIS special grade) was slowly layered along the inside wall of the bottle onto an equal volume of fullerene-saturated toluene solution to form a liquid–liquid interface. After forming the interface, the bottle was manually mixed 30 times, then kept still at 15 °C (SANYO MIR-153) for 5 days to complete fullerene precipitation. Then, the supernatant was removed, and 2-propanol was poured into the glass bottle to stabilize the precipitates. After vacuum filtration (KIRIYAMA 5B-21, ULVAC DTC-21), the precipitates were vacuum-dried (AS ONE VO-300) at room temperature.

Structural analysis of specimens was performed by XRD (Rigaku Ultima III) and a FIB-SEM (Hitachi NB5000) equipped with a Ga ion beam source and a field-emission scanning electron microscope (FE-SEM).

Chemical compositions of the specimens was analyzed by HPLC (JASCO UV-2070, PU 2089, CO-2065, LC-Net II/ADC) and Raman spectrometry (JASCO NRS-3000).

The optical properties of the specimens were investigated by ultraviolet–visible spectroscopy (UV–vis, JASCO V-570). The measurement was performed for the vacuum-dried powder of FNWs by the diffuse reflection method using an integrating sphere.

3. Results and discussion

The mother solutions were analyzed by HPLC, the chemical composition of each mother solution was determined.

Fig. 1 shows optical microscope images of the synthesized precipitates with various morphologies and metallic lusters. The images show the formation of fine needle-like crystals (nano-whiskers) in (a), (b) and (f), much bigger needle-like crystals in (c) and (d) and fine granular precipitates in (e).

Fig. 2 shows X-ray diffraction patterns of synthesized C_{60}NWs (a) and of C_{60}–C_{70}NWs synthesized using a mother solution with a composition of C_{60}–24 mass% C_{70} (b). Peaks corresponding to a face-centered cubic (fcc) phase and a triclinic (tr) phase can be assigned in the C_{60}NWs. It is likely that the tr phase was formed by distortion of the fcc phase [28]. The lattice constant of the fcc phase was determined to be $a=1.422\pm0.005$ nm. Peaks corresponding to a rhombohedral phase (rh) in addition to the fcc phase and the tr phase were also observed in the C_{60}–C_{70}NWs. It has been reported that C_{60} can be transformed to a polymer with an rh phase by

Table 1
Lattice constants of C_{60}NWs and C_{60}–C_{70}NWs.

Specimens	Crystal system	Lattice constant (nm)	Primitive unit cell volume (nm^3)
C_{60}NWs	Face-centered cubic (fcc)	$a=1.422\pm0.005$	0.719
	Triclinic (tr)	$a=0.950$, $b=1.000$ $c=1.010$, $\alpha=74.9°$ $\beta=59.4°$, $\gamma=60.0°$	0.715
C_{60}–C_{70}NWs	fcc	$a=1.433\pm0.011$	0.736
	tr	$a=0.951$, $b=0.954$ $c=1.018$, $\alpha=75.4°$ $\beta=60.0°$, $\gamma=60.0°$	0.693
	Rhombohedral (rh)	$a=1.174$, $c=1.652$	0.657

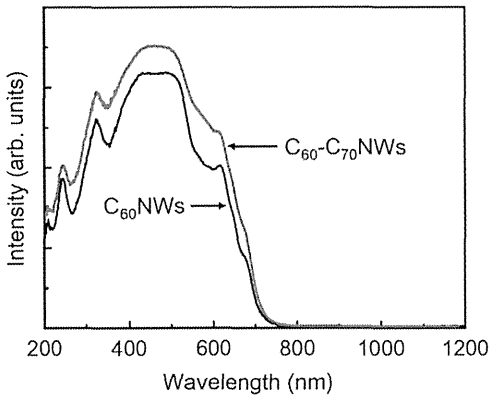

Fig. 3. UV–vis spectra of the C_{60}NWs and the C_{60}–C_{70}NWs obtained using a mother solution with a composition of C_{60}–24 mass% C_{70}.

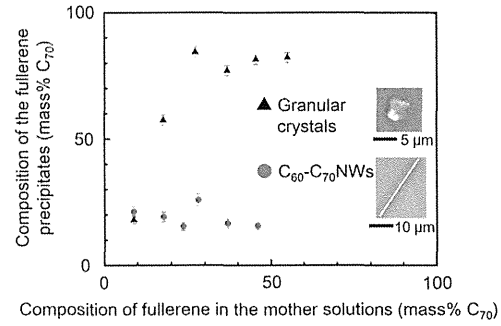

Fig. 4. Chemical composition of the granular crystals and the C_{60}–C_{70}NWs determined by Raman spectroscopy.

high-temperature high-pressure treatment [29]. It is likely that partial polymerization of C_{60} molecules was caused by the addition of C_{70} molecules. The lattice constant of the fcc phase was determined to be $a=1.433\pm0.011$ nm, 0.77% larger than the C_{60}NW lattice constant ($a=1.422\pm0.005$ nm). Table 1 shows the lattice constants and primitive unit cell volumes of C_{60}NWs and C_{60}–C_{70}NWs.

Fig. 3 shows the UV–vis absorption spectra of C_{60}NWs and C_{60}–C_{70}NWs synthesized using a mother solution with a composition of C_{60}–24 mass% C_{70}. The hyperchromic effect and a bathochromic shift were observed for the C_{60}–C_{70}NWs compared to the C_{60}NWs. The C_{60}–C_{70}NWs have a wider light absorption band than the C_{60}NWs, showing stronger absorption especially around 600 nm. This is caused by the wider and stronger absorption range of C_{70} than C_{60} [30].

The composition of C_{60}–C_{70} two-component specimens was measured by Raman spectroscopy and calculated using the peak area ratios, $100\times S_2/(S_1+S_2)$, where S_1 is the peak area of $A_g(2)$ and S_2 is the peak area of $A_1'(6)$ [31]. A linear relationship was assumed to hold between the peak area ratio and the fullerene composition (mass% C_{70}).

Fig. 4 shows the chemical composition of the C_{60}–C_{70}NW surfaces and the granular precipitates as determined by Raman spectroscopy. When the composition of fullerene in the mother solution is 9 mass% C_{70}, the granular precipitates and the C_{60}–C_{70}NWs have similar compositions. However, when the composition of fullerene in the mother solution is at least 18 mass% C_{70}, the composition of fullerene (mass% C_{70}) in the granular crystals is much higher than in the C_{60}–C_{70}NWs. It is likely that the granular precipitates are rich in C_{70} precipitate when the fullerene composition (mass% C_{70}) in the mother solutions exceeds the solid solubility limit of C_{70} in the C_{60} matrix phase.

Chemical composition analysis for the supernatant solutions was performed as shown in Fig. 5. This figure can be divided into three regions (I, II, III). The boundary between I and II is located at 12.4 mass% C_{70}, and the boundary between II and III is located at 73.4 mass% C_{70}. Fig. 5 indicates that the solid solubility of C_{70} in the matrix phase of C_{60} is 12.4 mass% and that the solid solubility of C_{60} in the matrix phase of C_{70} is 26.6 mass%. The chemical compositions of the precipitates determined by HPLC are shown in Fig. 6. Fig. 5 shows that C_{70} is unsaturated in the supernatant solutions for compositions ranging from 0 mass% C_{70} to 12.4 mass% C_{70}, corresponding to region I of Fig. 6. Fig. 5 also shows that C_{60} is unsaturated in the supernatant solutions for compositions ranging from 73.4 mass% C_{70} to 100 mass % C_{70}, corresponding to region III of Fig. 6. Both C_{60} and C_{70} are saturated in the supernatant solutions for compositions ranging from 12.4 mass% C_{70} to 73.4 mass% C_{70}, corresponding to region II of Fig. 6.

Table 2 shows the chemical compositions of the thick C_{60}–C_{70} needle-like crystals determined by HPLC. HPLC analyses of the thick needle-like crystals were performed on individual crystals selected using fine probes. Thick C_{60}–C_{70} needle-like crystals contain 11.1 ± 2.2 mass% C_{70}, up to 13.7 mass% C_{70}. It was found that the solid solubility of C_{70} in the matrix phase of C_{60} is 13.7 mass%. This result corresponds with the result from Fig. 5 (12.4 mass%) as well as previous reports [32,33].

Fig. 7 shows SEM images of a fracture process for a thick C_{60}–C_{70} needle-like crystal synthesized using the mother solution with a composition of C_{60}–45 mass% C_{70}. Image (a) shows a notch formed by sputtering with Ga ion beams and a fixed part by deposition of tungsten (W). In images (b), (c) and (d), the C_{60}–C_{70} needle-like crystal was slowly bent by a molybdenum probe and fractured.

Fig. 8 shows SEM images of the fracture surfaces of the C_{60}–C_{70} needle-like crystals. The areas surrounded by the red lines are the areas measured for chemical composition by Raman spectroscopy. Fig. 9 shows the fullerene composition of the fractured surfaces. The fractured surfaces exhibited sinusoidally modulated compositions.

Spinodal decomposition is a phenomenon involving spontaneous biphasic separation, with a sinusoidally modulated structure occurring after a finite time. We believe that these modulated structures result from spinodal decomposition. In Fig. 9, the wavelength of spinodal decomposition is 7.44 ± 2.45 μm. The diffusion length must be comparable to half of the wavelength of spinodal decomposition (3.72 μm). The diffusion length was calculated based on the following equation [34–36]:

$$L=\sqrt{D\times t},\quad D=\frac{1}{6}\times\lambda^2\times\beta\times\nu_0\times\exp\left(-\frac{Q}{RT}\right),\quad \beta=\exp\left(\frac{S}{k_B}\right)$$

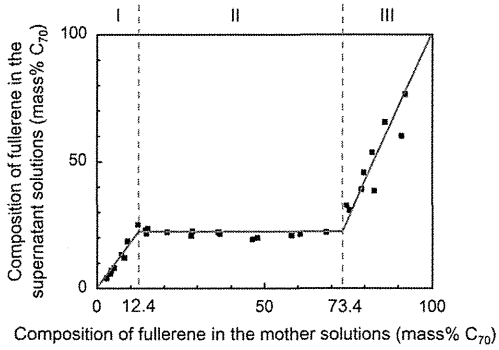

Fig. 5. Chemical composition of the supernatant solutions determined by HPLC.

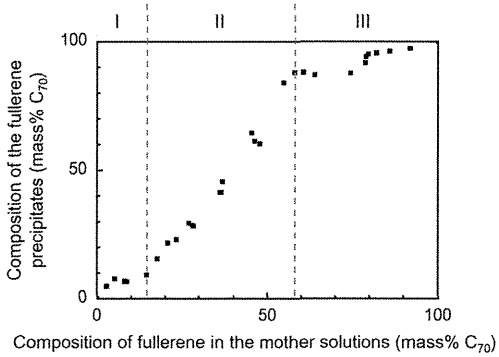

Fig. 6. Chemical composition of the precipitates determined by HPLC.

Table 2
Chemical composition of the thick C_{60}–C_{70} needle-like crystals analyzed by HPLC.

	Mother solution	Thick C_{60}–C_{70} needle-like crystals	
		Average	Maximum
Composition of fullerene (mass% C_{70})	45.4 ± 4.1	11.1 ± 2.2	13.7

where L is the average diffusion length. t is diffusion time, which is 5 days in the present paper. D is the diffusion coefficient. λ is the particle migration length, which is calculated to be $1.433/\sqrt{2}=1.013$ nm using the lattice constant from Table 1. β is the number of microscopic states and v_0 is the particle vibration frequency. R is the gas constant. S is the entropy and k_B is Boltzmann constant. Q is the activation energy of diffusion, which is equivalent to the binding energy between particles. $L=0.008596\times\exp(-Q/4789)$ [m], assuming $\beta=1$ and $v_0=10^9\ s^{-1}$ for $T=15$ °C. When L equals 3.72 μm, Q is calculated to be 37.1 kJ/mol from Fig. 10.

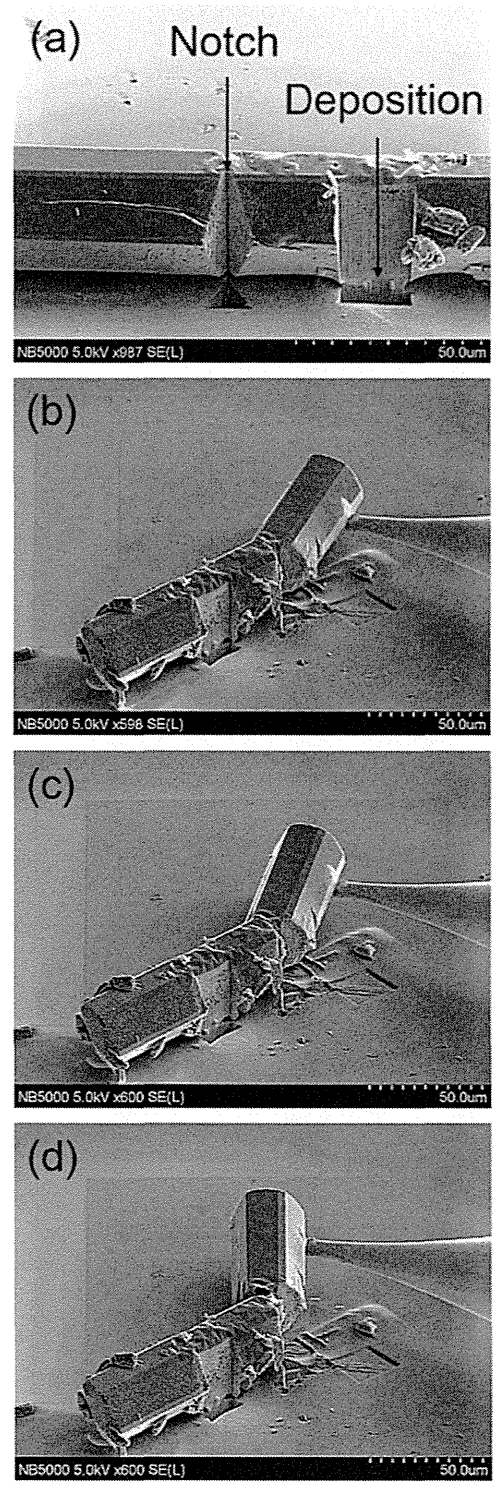

Fig. 7. SEM images of the fracture process of a C_{60}–C_{70} two-component needle-like crystal.

4. Conclusions

(1) The C_{60}–C_{70}NWs contained a small amount of rhombohedral phase and showed an fcc lattice constant that is 0.77% larger than that of C_{60}NWs.
(2) The C_{60}–C_{70}NWs showed a stronger visible light absorption than C_{60}NWs, especially at 600 nm.
(3) Both C_{60} and C_{70} are saturated in the supernatant solutions when the composition of fullerene in the mother solutions ranges from 12.4 mass% C_{70} to 73.4 mass% C_{70}.
(4) The solid solubility limit of C_{70} in the matrix phase of C_{60} is 13.7 mass%.
(5) C_{70} molecules precipitate as granular crystals when the concentration of C_{70} in the mother solutions exceeds the solid solubility limit of C_{70} in C_{60}.
(6) The fractured surfaces of C_{60}–C_{70} needle-like crystals showed modulated structures and chemical compositions, indicating spinodal decomposition. The activation energy of diffusion was calculated to be 37.1 kJ/mol.

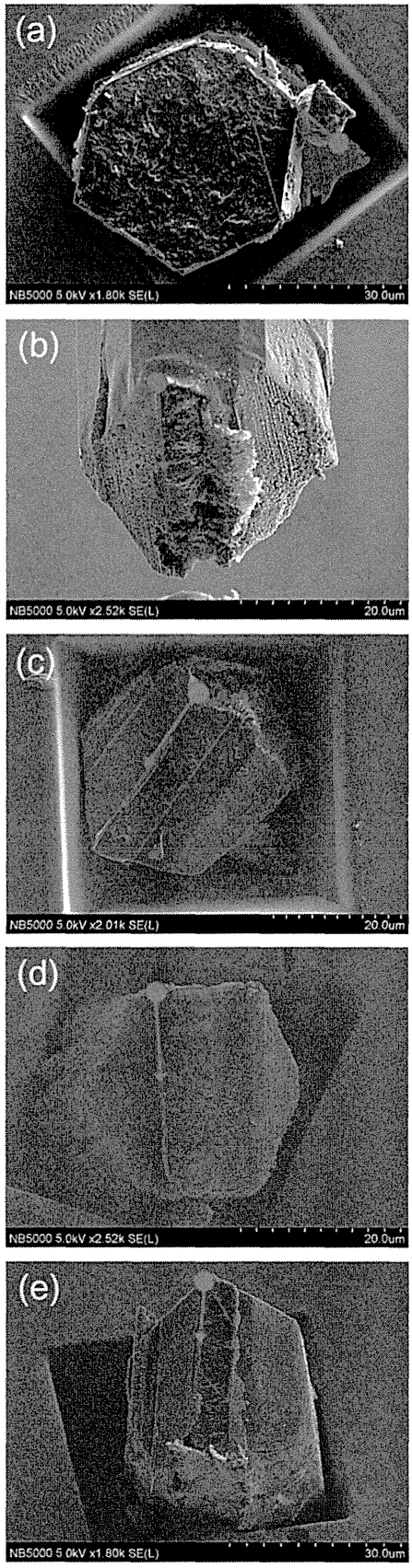

Fig. 8. SEM images of the fractured cross-sections of C_{60}–C_{70} two-component needle-like crystals. The areas surrounded by red lines were measured by Raman spectroscopy. (For interpretation of the references to color in this figure legend, the reader is referred to the web version of this article.)

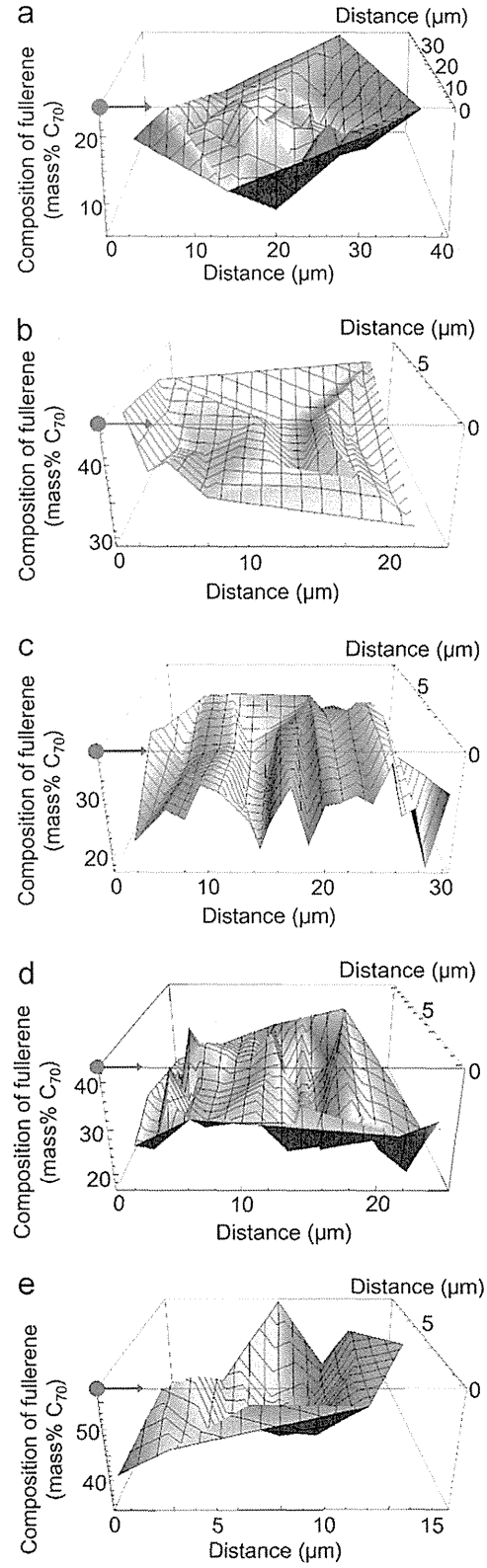

Fig. 9. Chemical composition of the fractured cross-sections of C_{60}–C_{70} needle-like crystals. (a)–(e) in the figure correspond to (a)–(e) in Fig. 8, respectively. The red arrows and circles in the figure correspond to those in Fig. 8. (For interpretation of the references to color in this figure legend, the reader is referred to the web version of this article.)

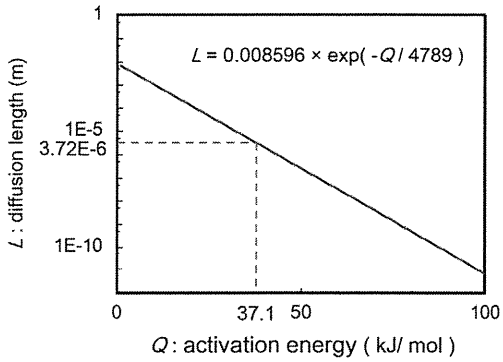

Fig. 10. Relationship between the diffusion length and the activation energy of C_{60} molecules calculated using $t=5$ days, $\lambda=1.013$ nm, $\beta=1$, $\nu_0=10^9\ s^{-1}$ and $T=15$ °C.

Acknowledgments

Portions of this research were supported by the Health and Labor Sciences Research Grants (H24-Chemistry-Shitei-009) from the Ministry of Health, Labor and Welfare of Japan, the JST Strategic Japanese-EU Cooperative Program "Study on managing the potential health and environmental risks of engineered nanomaterials", the Center of Materials Research for Low Carbon Emission of NIMS, and JSPS KAKENHI Grant number 26600007.

References

[1] H.W. Kroto, J.R. Heath, S.C. O'Brien, R.F. Curl, R.E. Smalley, Nature 318 (1985) 162–163.
[2] R.E. Haufler, J. Conceicao, L.P.F. Chibante, Y. Chai, N.E. Byrne, S. Flanagan, M.M. Haley, S.C. O'Brien, C. Pan, Z. Xiao, W.E. Billups, M.A. Ciufolini, R. H. Hauge, J.L. Margrave, L.J. Wilson, R.F. Curl, R.E. Smalley, J. Phys. Chem. 94 (1990) 8634.
[3] W. Krätschmer, L.D. Lambt, K. Fostiropoulos, D.R. Huffmant, Nature 347 (1990) 354.
[4] H. Ajie, M.M. Alvarez, S.J. Anz, R.D. Beck, F. Diedrich, K. Fostiropoulos, D.R. Huffman, W. Krätschmer, Y. Rubin, K.E. Shriver, D. Sensharma, R. L. Whetten, J. Phys. Chem. 94 (1990) 8630.
[5] J.B. Howard, J.T. McKinnon, M.E. Johnson, Y. Makarovsky, A.L. Lafleur, J. Phys. Chem. 96 (1992) 6657.
[6] J.B. Howard, J.T. McKinnon, Y. Makarovsky, A.L. Lafleur, M.E. Johnson, Nature 352 (1991) 139.
[7] Fullerene Nanowhiskers, in: K. Miyazawa (Ed.), Pan Stanford Publishing Pte. Ltd, Singapore, 2011.
[8] K. Miyazawa, J. Nanosci. Nanotechnol. 9 (2009) 41–50.
[9] K. Miyazawa, A. Obayashi, M. Kuwabara, J. Am. Ceram. Soc. 84 (2001) 3037–3039.
[10] K. Rauwerdink, J. Liu, J. Kintigh, G.P. Miller, Microsc. Res. Tech. 70 (2007) 513.
[11] K. Miyazawa, Y. Kuwasaki, A. Obayashi, M. Kuwabara, J. Mater. Res. 17 (2002) 83–88.
[12] K. Ogawa, T. Kato, A. Ikegami, H. Tsuji, N. Aoki, Y. Ochiai, J.P. Bird. Appl. Phys. Lett. 88 (2006) 112109.
[13] P.R. Somani, S.P. Somani, M. Umeno, Appl. Phys. Lett. 91 (2007) 173503.
[14] K. Miyazawa, J. Minato, H. Zhou, T. Taguchi, I. Honma, T. Suga, J. Eur. Ceram. Soc. 26 (2006) 429.
[15] Q. Wang, Y. Zhang, K. Miyazawa, R. Kato, K. Hotta, T. Wakahara, J. Phys. Conf. Ser. 159 (2009) 012023.
[16] M. Sathish, K. Miyazawa, T. Sasaki, Chem. Mater. 19 (2007) 2398.
[17] M. Sathish, K. Miyazawa, T. Sasaki, J. Solid State Electrochem. 12 (2008) 835.
[18] M. Sathish, K. Miyazawa, T. Sasaki, Diamond Relat. Mater. 17 (2007) 571.
[19] M. Sathish, K. Miyazawa, Nano 3 (19) (2008) 409.
[20] B.H. Cho, K.B. Lee, K. Miyazawa, W.B. Ko, Asian J. Chem. 25 (2013) 8027.
[21] X. Zhang, Y. Qu, G. Piao, J. Zhao, K. Jiao, Mater. Sci. Eng., B 175 (2010) 159.
[22] K. Asaka, T. Nakamura, K. Miyazawa, Y. Saito, Surf. Interface Anal. 44 (2012) 780.
[23] H. Takeya, K. Miyazawa, R. Kato, T. Wakahara, T. Ozaki, H. Okazaki, T. Yamaguchi, Y. Takano, Molecules 17 (2012) 4851.
[24] H. Takeya, R. Kato, T. Wakahara, K. Miyazawa, T. Yamaguchi, T. Ozaki, H. Okazaki, Y. Takano, Mater. Res. Bull. 48 (2013) 343.
[25] K. Asaka, R. Kato, K. Miyazawa, T. Kizuka, Appl. Phys. Lett. 89 (2006) 071912.
[26] K. Miyazawa, M. Fujino, J. Minato, T. Yoshii, T. Kizuka, T. Suga, Structure and properties of fullerene nanowhiskers prepared by the liquid–liquid interfacial precipitation method, in: Proc. SPIE 5648, Smart Materials III, P. 224, Smart Materials, Nano-, and Micro- Smart Systems 2004, 12–15 December 2004, Sydney, Australia.
[27] D. Matsuura, T. Konno, T. Wakahara, K. Miyazawa, T. Kizuka, Young's modulus of C_{60}/C_{70} alloy nanowhiskers, in: Abstracts of 2014 Tsukuba Nanotechnology Symposium (TNS'14), July 25–26, 2014, University of Tsukuba, Tsukuba, Japan.
[28] K. Miyazawa, H. Satsuki, M. Kuwabara, M. Akaishi, J. Mater. Res., 16 (2001) 1960.
[29] Y. Iwasa, T. Arima, R.M. Fleming, T. Siegrist, O. Zhou, R.C. Haddon, L.J. Rothberg, K.B. Lyons, H.L. Carter Jr., A.F. Hebard, R. Tycko, G. Dabbagh, J.J. Krajewski, G.A. Thomas, T. Yagi, Science 264 (1994) 1570.
[30] S. Pfuetzner, J. Meiss, A. Petrich, M. Riede, K. Leo, Appl. Phys. Lett. 94 (2009) 223307.
[31] R. Meilunas, R.P.H. Chang, S. Liu, M. Jensen, M.M. Kappes, J. Appl. Phys. 70 (1991) 5128.
[32] D. Havlik, W. Schranz, M. Haluška, H. Kuzmany, P. Rogl, Solid State Commun. 104 (1997) 775.
[33] K. Miyazawa, J. Minato, J. Mater. Res. 20 (2005) 688.
[34] M. Vos, P.L. Grande, D.K. Venkatachalam, S.K. Nandi, R.G. Elliman, Phys. Rev. Lett. 112 (2014) 175901.
[35] S. Kawasaki, E. Sakai, J. Nucl. Sci. Technol. 4 (1967) 273.
[36] E. Fujita, Kinzoku Butsuri -Zairyou Kagaku no Kiso-, Agne 661 (1996) (in Japanese).

The Journal of Toxicological Sciences (J. Toxicol. Sci.)
Vol.39, No.2, 363-370, 2014

Original Article

Teratogenicity of asbestos in mice

Tomoko Fujitani[1], Motoki Hojo[1], Akiko Inomata[1], Akio Ogata[1], Akihiko Hirose[2], Tetsuji Nishimura[3] and Dai Nakae[1]

[1]*Department of Pharmaceutical and Environmental Sciences, Tokyo Metropolitan Institute of Public Health, 3-24-1, Hyakunincho, Shinjuku-ku, Tokyo 169-0073, Japan*
[2]*Division of Risk Assessment, Biological Safety Research Center, National Institute of Health Science, 1-18-1, Kamiyoga, Setagaya-ku, Tokyo 158-8501, Japan*
[3]*Department of Pharmacology, Teikyo Heisei University, 4-21-2, Nakano, Nakano-ku, Tokyo 164-8530, Japan*

(Received January 14, 2014; Accepted February 14, 2014)

ABSTRACT — Possible teratogenicity of 3 different asbestos (crocidolite, chrysotile and amosite) was assessed in CD1(ICR) mice. Dams on day 9 of gestation were given a single intraperitoneal administration at dose of 40 mg/kg body weight of asbestos suspended in 2% sodium carboxymethyl cellulose solution in phosphate buffered saline, while dams in the control group were given vehicle (10 ml/kg body weight). Dams and fetuses were examined on day 18 of gestation. To compare with the control group, the mean percentage of live fetuses in implantations in the group given crocidolite and the incidence of dams with early dead fetuses in the groups given chrysotile or amosite were increased. While no external or skeletal malformation was observed in the control group, the incidence of external malformation (mainly reduction deformity of limb) in the group given amosite, and the incidences of skeletal malformation (mainly fusion of vertebrae) in the all dosed groups were significantly increased. The result indicated that asbestos (crocidolite, chrysotile and amosite) have fetotoxicity and teratogenicity in mice.

Key words: Teratogenicity, Asbestos, Crocidolite, Chrysotile, Amosite, Mice

INTRODUCTION

In the 20th century, asbestos had been widely utilized as a heat-proofing, fire-proofing and insulating material for inner coating of buildings and ships or in the electrical products. From late 1960's, hazards of asbestos became evident in humans (Selikoff and Hammond, 1968; Sheers and Templeton, 1968; Knox *et al.*, 1968) and experimental animals (Shin and Firminger, 1973; Pott *et al.*, 1974). The asbestos exposure induced lung fibrosis, lung cancer and, especially, delayed malignant mesothelioma not only in the workers of industries dealing with asbestos by the occupational exposure but also in the family members of such workers by the domestic exposure (Wasserman *et al.*, 1980; Miller, 1979). In Japan, the manufacture of asbestos fibers and of products used asbestos was prohibited, with some special exceptions, in 2006 and was completely prohibited in 2011 by the Ministry of Health, Labor and Welfare of Japan. However, the sufferers from asbestosis may increase even in the future, because the malignant mesothelioma development by asbestos exposure has a long latency (20-55 years) in humans. And the great attention should be paid regarding on hazards of asbestos in the dust that will be released during the demolition of buildings and ships lined by asbestos in the past.

Recently, the induction of mesothelioma by multi-wall carbon nanotubes (MWCNT), a non-mineral asbestos-like fiber, has been reported in mice (Takagi *et al.*, 2008) and rats (Sakamoto *et al.*, 2009). Since then, the similarity and difference of carcinogenic events induced by those exogenous fibers have been enthusiastically discussed (Donaldson *et al.*, 2010; Schinwald *et al.*, 2012). On the other hand, during the course of toxicological evaluation for MWCNT, we have revealed the teratogenicity of MWCNT given intraperitoneally or intratracheally to mice (Fujitani *et al.*, 2012). And we are strongly interested in the possible teratogenicity of other fibrous materials, especially of asbestos, because the transplacental transfer of asbestos fibers into embryos were evident in humans and experimental animals (Cunningham and Pontefract, 1974; Haque *et al.*, 1992, 1998 and 2001;

Correspondence: Tomoko Fujitani (E-mail: Tomoko_Fujitani@member.metro.tokyo.jp)

Haque and Vrazel, 1998). To the best of our knowledge, there are no data available so far in the literature to describe either the presence or absence of the teratogenicity of asbestos. In this context, the present study was carried out to assess possible teratogenicity of asbestos, crocidolite, chrysotile and amosite, in mice.

MATERIALS AND METHODS

Ethical consideration of the experiment

An experimental protocol was approved by the Experiments Regulation Committee and the Animal Experiment Committee of the Tokyo Metropolitan Institute of Public Health prior to its execution and monitored at every step during the experimentation for its scientific and ethical appropriateness, including concern for animal welfare, with strict obedience to the National Institutes of Health Guideline for the Care and Use of Laboratory Animals, Japanese Government Animal Protection and Management Law, Japanese Government Notification on Feeding and Safekeeping of Animals and other similar laws, guidelines, rules *et cetera* provided domestically and internationally.

Test chemicals

Crocidolite, chrysotile and amosite (all chemically pure and pretreated Union Internationale Centre le Cancer (UICC)), were autoclaved (120°C, 30 min) for the sterility and were suspended in sterilized 2% sodium carboxymethyl cellulose (Tokyo Chemical Industry Co., Ltd., Tokyo, Japan) /phosphate buffered saline by vigorous stirring and sonication, to gain the uniform suspension.

Animals

Specific pathogen free female Crlj: CD1(ICR) mice, on gestational days 3, 4, 7 or 8 (the day with vaginal plug at the morning after housing with male was regarded as day 0), were purchased from Charles River Japan Inc. (Kanagawa, Japan) and were housed individually in plastic cages with cedar chip bedding and allowed free access to the standard diet CE2 (Nihon Clea, Inc., Tokyo, Japan) and water. The animal room was maintained at 23-25°C with a relative humidity of 50-60%, with 10 ventilations per hour (drawing fresh air through an HEPA-filter, 0.3 μm, 99.9% efficiency) and on a 12 hr light/dark cycle.

Experiment

On day 9 of gestation, dams were randomly allocated to 4 groups by body weights and were given a single intraperitoneal administration of asbestos at the dose of 40 mg/10 ml/kg body weight. The control mice were given vehicle. Body weights and food consumptions were measured daily and clinical observations were recorded. Relative food consumptions were calculated by dividing the absolute food consumption by the body weight (g/kg body weight/day). On day 18 of gestation, dams were anesthetized by diethyl ether and blood samples were collected in EDTA2K-anticoagulant tubes from the femoral vein. The white blood cell counts were examined by an auto-blood analyzer SYSMEX KX21-NV (SYSMEX, Kobe, Japan). Blood films were made, stained by Diff-Quik (SYSMEX) and counted for the subtypes of white blood cells under the light microscopy. Livers, kidneys, spleens and adrenals of dams were weighed. Uteri were opened, and the numbers and positions of implantation sites, early dead fetuses (defined as a case showing the implanted site and amorphous mass), late dead fetuses (defined as a case showing head and limbs) and live fetuses were examined. The numbers of corpora lutea in ovaries were also examined. Each live fetus was weighed and examined for external anomalies. Fetuses, of which internal organs in the peritoneal and thoracic cavities were carefully removed, were fixed in 95% ethanol for more than 1 week, soaked in 0.5% KOH for 24 hr, in 0.002% Alizarin Red S/ 0.5% KOH for 24 hr, in 0.4% KOH/20% Glycerin for 24 hr, in 50% Glycerin for more than 24 hr and examined for skeletal anomalies.

Statistical analysis

Scheffe's multiple comparison was applied for body weight of dam, food consumption of dam, number of implantations, number of early or late dead fetuses, number of live fetuses, and mean fetal body weights in each dam. The incidence of dams with early dead fetuses, late dead fetuses or malformed fetuses in dams in the groups and the incidence of malformed fetuses in the fetuses in the group were analyzed using the Chi square test.

RESULT

Dams did not die from the administration of asbestos in the current experimental conditions. Body weights of dams on 1 to 2 days after the administration of crosidolite, on 1 to 5 days after the administration of chrysotile, on 1 day after administration of amosite were significantly lower than that of the control group (Fig. 1). Absolute and relative food consumptions on 1 day after the administration of crocidolite, chrysotile and amosite were significantly lower than that of the control group (data not shown). Immediately after the administration to about 1

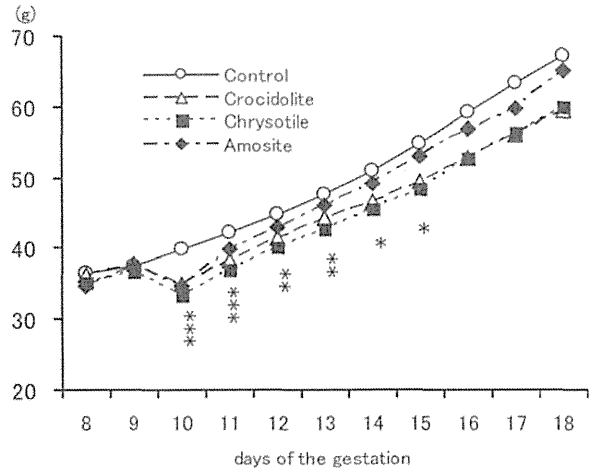

Fig. 1. Body weight gains of dams.

day after, dams given asbestos seemed less active than those of the control group. Effects of asbestos on dams are summarized in Table 1. Liver and spleen weight of dams in the group given crocidolite or amosite were significantly higher than those of the control group, while weights of kidneys and adrenals were not changed by administration of asbestos. The total white blood cell counts and the neutrocyte counts of dams in the group given crocidolite or amosite were significantly higher than that of the control group. In addition, monocyte counts of dams in the group given amosite was also significantly higher than that of the control group.

Pregnant statuses of dams are presented in Table 2. Most of the mated mice were gestated and had living fetuses regardless to the administration of asbestos. There was no statistical difference between control and dosed groups on the numbers of corpora lutea, implantation sites, early or late fetal death and live fetuses. However, the incidence of dams with early dead fetuses in groups given chrysotile or amosite was significantly increased to compare with that of the control group. Also, the percentage of live fetuses in the implantation sites of the group given crocidolite was significantly lower than that of the control group. The incidence of dams with late dead fetuses was not changed by administration of asbestos. Body weight of live fetuses (male and female) was not changed by administration of asbestos.

Incidences of malformation are presented in Table 3. The incidences of dams with fetuses having external malformations and the incidences of fetuses with external malformations were both significantly increased in the group given amosite. Observed external malformations included cleft face (Fig. 2), reduction deformity of limb (absence of finger or of forelimb) (Fig. 3), omphalocele, absent genital tubercule and absent tail (Fig. 4). Among those malformations, the incidence of the reduction deformity of limb significantly increased in the group

Table 1. Effects of intraperitoneal dose of asbestos on dams.

	Control	Asbestos dosed (40 mg/kg b.w.)		
	(CMCNa)	Crocidolite	Chrysotile	Amosite
Number of dams	9	10	9	10
Body weight (g) on day 9 of gestation	37.48 ± 2.07	37.89 ± 1.06	36.64 ± 1.75	37.64 ± 1.97
on day 18 of gestation	67.04 ± 6.02	59.54 ± 8.73	60.02 ± 6.92	65.14 ± 8.23
Organ weight				
Liver (g)	3.00 ± 0.24	3.83 ± 0.53***	3.41 ± 0.18	3.90 ± 0.32***
Kidney (mg)	458 ± 54	490 ± 51	441 ± 61	500 ± 21
Spleen (mg)	137 ± 20	422 ± 206***	266 ± 72	418 ± 126***
White blood cell count ($10^2/\mu l$)				
Total	42.5 ± 11.1	85.5 ± 31.4*	74.9 ± 19.5	101.5 ± 31.0***
Lymphocyte	31.7 ± 8.8	29.5 ± 10.1	30.2 ± 6.3	28.0 ± 6.7
Neutrocyte	9.6 ± 3.4	47.9 ± 21.7**	33.1 ± 12.2	64.0 ± 25.8***
Eosinocyte	0.4 ± 0.4	3.6 ± 3.0	7.4 ± 6.5	3.8 ± 2.1
Monocyte	0.8 ± 0.2	4.5 ± 3.4	4.2 ± 3.0	5.6 ± 3.3*

Values are the means ± standard deviations for numbers of dams in each group. Asterisks represent that the values are significantly different from the corresponding control values (*, ** or *** indicating $p < 0.05$, 0.01 or 0.001, respectively).

Table 2. Pregnant status of mice given Asbestos intraperitoneally on day 9 of the gestation

Reproductive parameters	Control	Asbestos dosed (40 mg/kg b.w.)		
	(CMCNa)	Crocidolite	Chrysotile	Amosite
Females mated[1)]	10	10	10	10
Females gestated[2)]	9	10	9	10
Females with >1 live fetus	9	10	9	10
Corpora lutea/litter[#]	17.9 ± 1.8	19.3 ± 1.4	18.7 ± 1.3	18.5 ± 1.4
Implantations/litter[#]	14.6 ± 2.5	14.3 ± 1.6	14.2 ± 1.2	14.9 ± 1.4
Death of fetuses[3)#]				
Number of early dead fetuses	0.1 ± 0.3	5.1 ± 5.5	3.9 ± 4.3	3.2 ± 3.3
(% of implantations)	(0.9 ± 2.8)	(36.2 ± 38.9)	(26.5 ± 28.6)	(22.0 ± 23.2)
Females with early dead fetuses/examined	1/9	5/10	8/9**	8/10**
Number of late dead fetuses	0	0.2 ± 0.4	0	0.1 ± 0.3
(% of implantations)	(0.0)	(1.4 ± 3.0)	(0.0)	(0.7 ± 2.1)
Females with late dead fetuses/examined	0/9	2/10	0/9	1/10
Live fetuses/litter[#]	14.4 ± 2.7	9.2 ± 5.3	10.3 ± 3.9	11.6 ± 3.7
(% of implantations)	(99 ± 3)	(64 ± 36*)	(74 ± 29)	(77 ± 23)
Body weight of live fetuses (g)[#]				
Male	1.47 ± 0.08	1.42 ± 0.12	1.43 ± 0.04	1.39 ± 0.08
Female	1.39 ± 0.08	1.33 ± 0.09	1.35 ± 0.06	1.33 ± 0.08

[1)] Number of animals with vaginal plug.
[2)] Number of animals with implantation sites.
[3)] 'Early' was defined as a case showing the implanted sites and amorphous mass, while 'Late' was defined as a case showing the head and limbs.
[#] Values are the means ± standard deviations.
The percent resorption (early or late dead fetus) and fetal body weight were obtained by averaging the value for each litter.
Asterisks represent that the values are significantly different from the corresponding control values (*, ** or *** indicating $p < 0.05$, 0.01 or 0.001, respectively).

given amosite. One reduction deformity (lack of a finger) in the group given crocidolite and one open eyelid in the group given chrysotile were observed but there was no statistical significance in the increase of those incidences. The incidences of dams with fetuses having skeletal malformations in the group given chrysotile and amosite were significantly increased compared with the control group. The incidences of fetuses with skeletal malformations in the all groups given asbestos were significantly increased compared with that of the control group. Among the observed skeletal malformations, the incidence of fusion of vertebral bodies and arches (Fig. 5) in the all groups given asbestos were significantly increased. Also, the incidence of reduction deformity of limb (absence of finger bones, absence of arm bone and so on) in the group given amosite was statistically significant.

DISCUSSION

The intraperitoneal administration of crocidolite, chrysotile and amosite had teratogenic effects in mice. We conducted the experiment of administration in intraperitoneal cavity to avoid the stress to the dam in the intratracheal administration. However, the fact that intraperitoneal administration of MWCNT had equal teratogenicity to that of the intratracheal administration (Fujitani *et al.*, 2012) led to the potential teratogenicity of those asbestos in the intratracheal exposure. The dose level in the present experiment on asbestos was over 10-fold higher compared with that on MWCNT (Fujitani *et al.*, 2012) as based on the weight of substance tested. The asbestos are mineral fibers having density at 2.4 to 3.25 g/cm^3. In contrast, MWCNT, having inner diameter of 2-10 nm as a cylinder form of graphene sheet having vacant inner space, has a bulk density at 0.14 to 0.28 g/cm^3. So, the bulk of 4 mg

Table 3. Incidences of malformations in mice given asbestos on day 9 of gestation

	Control	Asbestos dosed (40 mg/kg b.w.)		
	(CMCNa)	Crocidolite	Chrysotile	Amosite
External malformation				
Number of litters with malformed fetus/examined (percentages in the parentheses)				
	0/9 (0)	1/10 (10)	1/9 (11)	4/10 (40)*
Percent incidence of malformations#	0	2.0 ± 6.3	0.9 ± 2.8	4.1 ± 5.5
Numbers of malformed fetuses/examined	0/130	1/92	1/93	5/116*
Numbers of fetuses with				
open eyelid	0	0	1	0
cleft face	0	0	0	1
reduction deformity of limb	0	1	0	4*
omphalocele	0	0	0	1
absent genital tubercle	0	0	0	1
absent tail	0	0	0	1
Skeletal malformation				
Number of litters with malformed fetuses/examined (percentages in the parentheses)				
	0/9 (0)	3/10 (30)	4/9 (44)*	7/10 (70)**
Percent incidence of malformations#	0	7.4 ± 12.0	11.2 ± 18.1	10.5 ± 8.6
Numbers of malformed fetuses/examined	0/130	6/92**	5/93**	13/116***
Numbers of fetuses with				
gnatho-dysplasia	0	0	0	1
fusion of vertebral body and arch	0	5**	5**	9**
fusion of rib	0	2	1	1
reduction deformity of limb	0	1	0	6**
kinked or absent tail	0	0	2	1

Values are the means ± standard deviations obtained by averaging the value for each dam.
Asterisks represent that the values are significantly different from the corresponding control values (*, ** or *** indicating $p < 0.05$, 0.01 or 0.001, respectively).

MWCNT was shown to be equal to the bulk of 40 mg asbestos fibers (Fig. 6). In the preliminary study on teratogenicity of asbestos, we did not observe any adverse effects of asbestos on dam and fetus in the dose level of 4 mg/kg body weight and the bulk of 4 mg of asbestos seems very little to compare with the 4 mg MWCNT (Fig. 7). The detailed dose-dependent profile of the teratogenicity of asbestos is now being assessed in our laboratories.

Winkler and Rüttner (1982) reported that numerous phagocytes were mobilized on the surface of the mesenteric tissue to engulf asbestos fibers given intraperitoneal cavity within 24 hr. We observed the grayish-colored and/or swollen lymph nodes beside the thymus in thoracic cavity of dams given asbestos (data not shown) in the same way observed in dams given MWCNT. It is thus likely to speculate that intraperitoneally administered asbestos fibers in the present study might at least partly be carried by lymphatic or blood flow from peritoneal cavity. Some literature indicates that transplacental distribution of asbestos from dam to fetus (Cunnibgham and Pontecraft, 1974; Haque *et al.*, 1992, 1998 and 2001; Haque and Vrazel 1998). So, asbestos fibers might penetrate past the placenta to embryos in the present study. As asbestos have cytotoxicity (Lipkin, 1980; Lock and Chamberlain, 1983) and genotoxicity (Libbus *et al.*, 1989; Marczynski *et al.*, 1994; Dopp *et al.*, 1997; Dopp and Schiffmann, 1998) on mammalian cells, rapidly proliferating embryonic cells may become an essential target of the asbestos toxicity. The result that the administration of chrysotile and amosite increased the

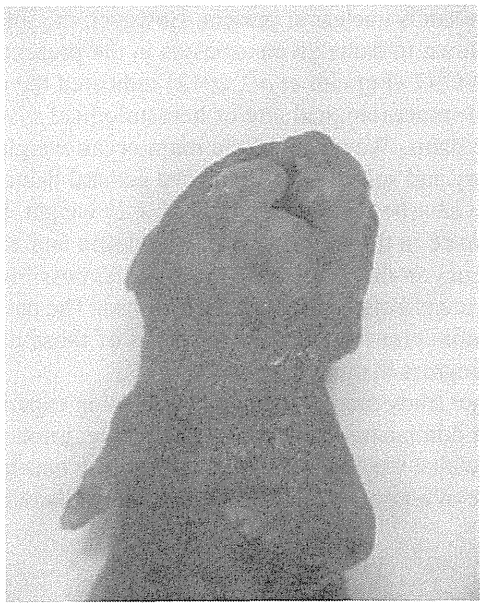

Fig. 2. Cleft face and reduction deformity of right forelimb shown in a fetus of the group given amosite.

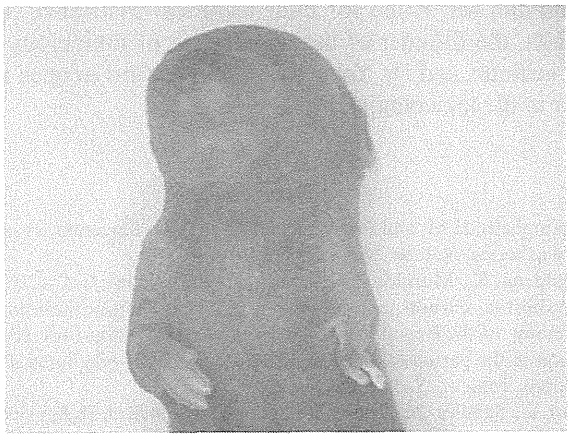

Fig. 3. Reduction deformity of right and left forelimbs shown in a fetus of the group given amosite.

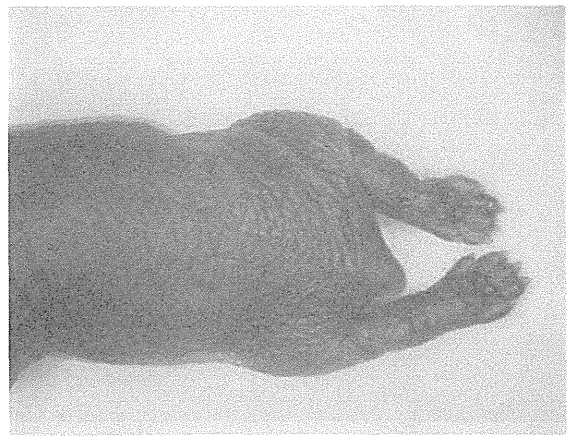

Fig. 4. Absence of tail shown in a fetus of the group given amosite.

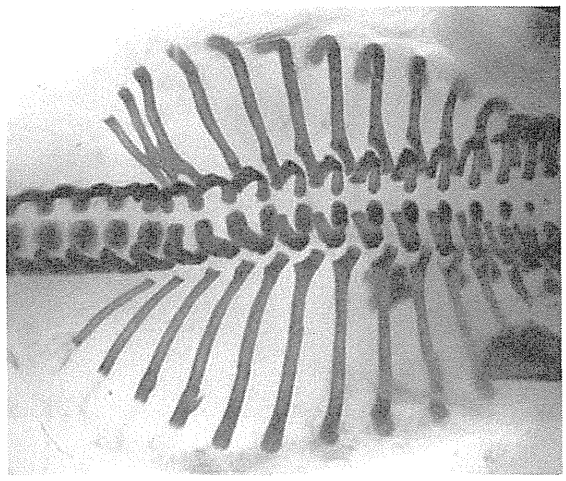

Fig. 5. Fusion of vertebrae and ribs shown in a fetus of the group given crocidolite.

incidence of dams with early dead fetus and the administration of crosidolite decreased the percentages of live fetuses in the implantation sites indicated the lethal damage(s) by asbestos on whole embryos. And, in the surviving fetuses, external and/or skeletal malformations were evident in the groups given asbestos. Gestational day 9 is the specific narrow window to cause the reduction deformity of limbs and tail in fetuses of mice given teratogenic chemicals (Ogata *et al.*, 1984). Although asbestos fibers were still observed macroscopically in the peritoneal cavity on day 18 of gestation, the adverse effect of asbestos on fetuses appeared to be restricted in the early stage of the organogenesis period, because late fetal death and weight of fetuses were not changed in the groups given asbestos. Another possible pathogenesis of exogenous fibers may be immuno-modulating and inflammatory effects. Pleural inflammation was targeted regarding on induction of mesothelioma by carbon nanotubes (Murphy *et al.*, 2012) and asbestos (Schinwald *et al.*, 2012). Yamaguchi *et al.* (2012) reported the stimulated immune and inflammatory responses from 1 to 20 weeks after intraperitoneal administration of MWCNT in female mice. In that study, effects of crocidolite were also examined to compare with those of MWCNT and the admin-

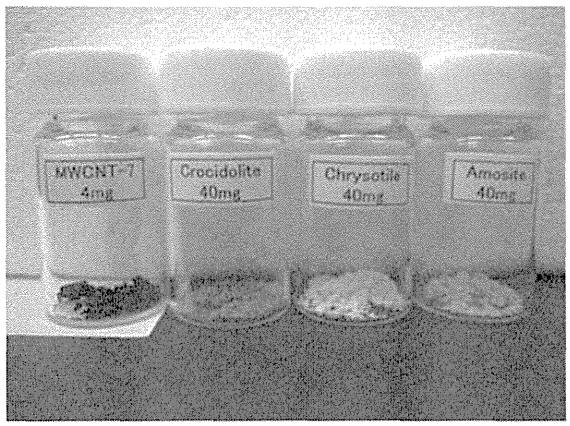

Fig. 6. Macroscopic appearance of Asbestos (40 mg) and MWCNT (4 mg).

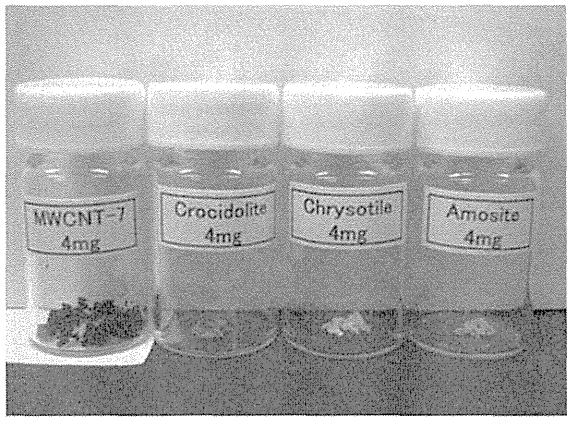

Fig. 7. Macroscopic appearance of Asbestos (4 mg) and MWCNT (4 mg).

istration of crocidolite fibers significantly increased the white blood cell counts, granulocyte counts and monocyto counts in peripheral blood at 1 week after the administration. In the present study, white blood cell counts were tended to increase in all the groups given asbestos, even though statistical significance was not apparent in the group given chrysotile. And the result of the present study indicated that the increase of white blood cell counts in dosed groups were due to the increase of neutrocyte counts. There was a tendency to increase eosinocyte counts and monocyte counts in the dosed groups but statistical significance was evident only in the monocyte counts in the amosite group. So, most striking change in white blood cell counts of dam given asbestos was the increase of neutrocytes. The relation between the immunological changes in dam and the defects of embryonal development is unclear at present. However, the splenomegaly shown in dams given asbestos in the present study and MWCNT (Fujitani *et al.*, 2012) indicated the disturbance of immunological and/or hematological system(s) in those dams. We weighed the main organ weight (liver, kidney and spleen) to monitor the general damages in dams given asbestos. The increase of liver weight, having significance in the groups given crocidolite and amosite or tendency in the group given chrysotile, possibly indicated acute effects on the liver by asbestos. The pathological examination on livers and spleens of those dams is under progress in our laboratory.

Further study might be required, including experiments by other administration routes, for example, intratracheal or oral which may be valuable to clarify the non-hazardous dose of teratogenic effects of asbestos in humans.

ACKNOWLEDGEMNTS

This work was supported in part by a research budget of the Tokyo Metropolitan Government, Japan, and a Grant-in-Aid from the Ministry of Health, Labor and Welfare of Japan. The authors gratefully thank to Mr. Ando and Mr. Kubo for their technical assistance, Dr. Hiraga, the founder of the department of toxicology in our institute, and Dr. Yoneyama, for her effort to open the door to the toxicologist for the first author.

REFERENCES

Cunningham, H.M. and Pontefract, R.D. (1974): Placental transfer of asbestos. Nature, **249**, 177-178.

Donaldson, K., Murphy, F.A., Duffin, R. and Poland, C.A. (2010): Asbestos, carbon nanotubes and the pleural mesothelium: A review of the hypothesis regarding the role of long fibre retention in the parietal pleura, inflammation and mesothelioma. Part Fibre. Toxicol., **7**, 5.

Dopp, E., Schuler, M., Schiffmann, D. and Eastmond, D.A. (1997): Induction of micronuclei, hyperdiploidy and chromosomal breakage affecting the centric/pericentric regions of chromosomes 1 and 9 in human amniotic fluid cells after treatment with asbestos and ceramic fibers. Mutat. Res., **377**, 77-87.

Dopp, E. and Schiffmann, D. (1998): Analysis of chromosomal alterations induced by asbestos and ceramic fibers. Toxicol. Lett., **96-97**, 155-162.

Fujitani, T., Ohyama, K., Hirose, A., Nishimura, T., Nakae, D. and Ogata, A. (2012): Teratogenicity of multi-wall carbon nanotube (MWCNT) in ICR mice. J. Toxicol. Sci., **37**, 81-89.

Haque, A.K., Mancuso, M.G., Williams, M.G. and Dodson, R.F. (1992): Asbestos in organs and placenta of five stillborn infants suggests transplacental transfer. Environ. Res., **58**, 163-175.

Haque, A.K. and Vrazel, D.M. (1998): Transplacental transfer of asbestos in pregnant mice. Bull. Environ. Contam. Toxicol., **60**, 620-625.

Haque, A.K., Vrazel, D.M. and Uchida, T. (1998): Assessment of

asbestos burden in the placenta and tissue digests of stillborn infants in South Texas. Arch. Environ. Contam. Toxicol., **35**, 532-538.

Haque, A.K., Ali, I. and Vrazel, D.M. (2001): Chrysotile asbestos fibers detected in the newborn pups following gavage feeding of pregnant mice. J. Toxicol. Environ. Health, Part A, **62**, 23-31.

Knox, J.F., Holmes, S., Doll, R. and Hill, I.D. (1968): Mortality from lung cancer and other causes among workers in an asbestos textile factory. Br. J. Ind. Med., **25**, 293-303.

Libbus, B.L., Illenye, S.A. and Craighead, J.E. (1989): Induction of DNA strand breaks in cultured rat embryo cells by crocidolite asbestos as assessed by nick translation. Cancer Res., **49**, 5713-5718.

Lipkin, L.E. (1980): Cellular effects of asbestos and other fibers: Correlations with *in vivo* induction of pleural sarcoma. Environ. Health Perspect., **34**, 91-102.

Lock, S.O. and Chamberlain, M. (1983): Cytotoxic action of mineral dusts on CHV 79 cells *in vitro*: Factors affecting toxicity. Environ. Health Perspect., **51**, 189-193.

Marczynski, B., Czuppon, A.B., Marek, W. Reichel, G. and Baur, X. (1994): Increased incidence of DNA double-strand breaks and anti-ds DNA antibodies in blood of workers occupationally exposed to asbestos. Hum. Exp. Toxicol., **13**, 3-9.

Murphy, F.A., Schinwald, A., Poland, C.A. and Donaldson, K. (2012): The mechanism of pleural inflammation by long carbon nanotubes: interaction of long fibres with macrophages stimulates them to amplify pro-inflammatory responses in mesothelial cells. Particle and Fibre Toxicology, **9**, 8.

Miller, R.W. (1979): Advances in understanding causes of childhood cancer. Pediatric Analis., **8**, 710-715.

Ogata, A., Ando, H., Kubo, Y. and Hiraga, K. (1984): Teratogenicity of thiabendazole in ICR mice. Food Chem. Toxic., **22**, 509-520.

Pott, F., Huth, F. and Friedrichs, K.H. (1974): Tumorigenic effect of fibrous dusts in experimental animals. Environmental Health Perspectives, **9**, 333-315.

Sakamoto, Y., Nakae, D., Fukumori, N., Tayama, K., Maekawa, A., Imai, K., Hirose, A., Nishimura, T., Ohashi, N. and Ogata, A. (2009): Induction of mesothelioma by a single intrascrotal administration of multi-wall carbon nanotube in intact male Fischer 344 rats. J. Toxicol. Sci., **34**, 65-76.

Schinwald, A., Murphy, F.A., Prina-Mello, A., Poland, C.A., Byrne, F., Movia, D., Glass, J.R., Dickerson, J.C., Schultz, D.A., Jeffree, C.E., MacNee, W. and Donaldson, K. (2012): The threshold length for fiber-induced acute pleural inflammation: Shedding light on the early events in asbestos-induced mesothelioma. Toxicol. Sci., **128**, 461-470.

Schneider, U. and Maurer, R.R. (1977): Asbestos and embryonic development. Teratology, **15**, 273-279.

Selikoff, I.J. and Hammond, E.C. (1968): Environmental epidemiology. 3. Community effects of nonoccupational environmental asbestos exposure. Am. J. Public Health Nations Health, **58**, 1658-1666.

Sheers, G. and Templeton, A.R. (1968): Effects of asbestos in dockyard workers. Br. Med. J., **3**, 574-579.

Shin, M.L. and Firminger, H.I. (1973): Acute and chronic effects of intraperitoneal injection of two types of asbestos in rats with a study of the histopathogenesis and ultrastructure of resulting mesotheliomas. Am. J. Pathol., **70**, 291-314.

Takagi, A., Hirose, A., Nishimura, T., Fukumori, N., Ogata, A., Ohashi, N., Kitajima, S. and Kanno, J. (2008): Induction of mesothelioma in p53+/- mouse by intraperitoneal application of multi-wall carbon nanotube. J. Toxicol. Sci., **33**, 105-116.

Wasserman, M., Wasserman, D. Steinitz, R., Katz, L. and Lemesch, C. (1980): Mesothelioma in children. IARC Sci. Publ., **30**, 253-257.

Winkler, G.C. and Ruttner, J.R. (1982): Penetration of asbestos fibers in the visceral peritoneum of mice. A scanning electron microscopic study. Exp. Cell Biol., **50**, 187-194.

Yamaguchi, A., Fujitani, T., Ohyama, K., Nakae, D., Hirose, A., Nishimura, T. and Ogata, A. (2012): effects of sustained stimulation with multi-wall carbon nanotubes on immune and inflammatory responses in mice. J. Toxicol. Sci., **37**, 177-189.